A PRACTICAL ALGORITHM FOR RECONSTRUCTION FROM X-RAY BACKSCATTER DATA

Young S. Ham and C.F. Poranski
Materials Chemistry Branch
Naval Research Laboratory
Washington DC 20375

E.C. Greenawald
Geo-Centers, Inc.
10903 Indian Head Highway
Ft. Washington MD 20744

INTRODUCTION

Although numerous applications of x-ray backscatter tomography (XBT) have been demonstrated, only a few have been fully developed to practical implementation [1-5]. In some applications the images produced by direct data acquisition and display methods are plagued with superposition artifacts that can interfere with interpretation [6]. Non-homogeneous materials such as composites or layered structures are particularly susceptible. Reconstruction methods have been proposed to correct the datum from each volume element (voxel) by exploiting the information in data from overlying voxels [7]. Practical inspection systems, however, present a more challenging problem than the monoenergetic highly collimated laboratory demonstration systems. In particular, the use of a *bremmstrahlung* source and a fan beam, or slit collimated, detector geometry, deprives us of knowledge of the backscattered photon energies and paths that are needed for a true reconstruction. In this paper, we present our work towards a reconstruction using data from a commercial XBT system (Philips ComScan) and a real composite inspection application. Our approach uses pre-processing to remove system artifacts, *a priori* information about the material, and an iterative method to determine the composition of each voxel.

METHODOLOGY

Our approach for the reconstruction is a semi-empirical method that utilizes *a priori* information about the sample. The object of study is sonar rubber dome (SRD), which consists of layers of steel cord reinforced rubber. A combination of several ideas is used to overcome the difficulties associated with the reconstruction

Review of Progress in Quantitative Nondestructive Evaluation, Vol. 15
Edited by D.O. Thompson and D.E. Chimenti, Plenum Press, New York, 1996

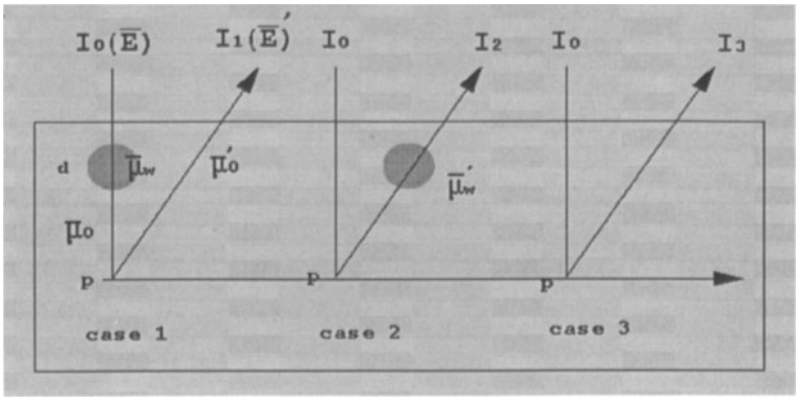

Figure 1: Schematic diagram to show the shadow artifacts due to the attenuation by incident and scattered beams. Darker circular shading represents material of higher density, i.e., steel cord in rubber matrix.

of SRD material. A simple normalization method is used to eliminate the need for calculation of detector efficiency, of solid angle at the scatter point subtended by a rectangular aperture, and of transmission efficiency through the fiber optics. The data obtained from the object is divided against data from a calibration sample, voxel by voxel. These are conveniently converted into 256 levels for visualization or further image processing. The ideal calibration sample for the SRD would be the rubber matrix material.

Ideally, the normalized data will show that the rubber has the relative density of unity regardless of depth, ignoring statistical errors. Of course, the shadow artifacts due to the attenuation by the cords would be still visible. Since the attenuation through the rubber was compensated by this normalization process, the problem of reconstruction is reduced to correctly quantify the amount of attenuation by both the primary and scattered beams.

Consider an XBT scan of a sample which contains a cord made of steel as shown in Figure 1. A pencil-beam is perpendicularly incident upon the sample, scattered at the point p and collected at the detector. Since the incident beam contains polyenergetic x-rays from an X-ray tube, $I_0(\overline{E})$ can be defined as

$$I_0(\overline{E}) = \int_{E_{min}}^{E_{max}} I_0(E)dE \tag{1}$$

where $\overline{E}$ is loosely defined as the effective energy of the x-ray tube. $I_1(\overline{E}')$ is the corresponding integrated intensity when $I_0(\overline{E})$ is scattered through an angle θ. In the notation of the linear attenuation coefficients, subscripts w and 0 stand for cord and the rubber matrix. The $'$ represents that the photons are scattered. If the linear attenuation coefficient of the matrix is different from that of the cord at effective energy $\overline{E}$, the intensities, I_1, I_2, and I_3, escaping from the sample corresponding to cases 1, 2, and 3, will be greatly different due to their different beam paths, even if the densities at the scatter sites are the same. Thus, in a practical situation, it would be difficult to recognize whether the difference is due to the

different beam path or to the different densities at the scatter site. Complete knowledge of the material above the point P is required in order to evaluate the densities at the scatter site. Assuming such information is available, we would like to calculate compensation factors such that the scattered intensities for cases 1 and 2 are equal to I_3. These compensation factors can be calculated by obtaining ratios of I_1 or I_2 to I_3. That is, the normalization can be used to obtain the compensation factors rather than calculating the absolute intensities for all 3 cases.

The compensation factor for the incident beam when it traverses a distance d, the diameter of the cord, can be shown to be

$$\frac{I_3(\overline{E}')}{I_1(\overline{E}')} = e^{(\overline{\mu}_w - \overline{\mu}_0)d} = \alpha \tag{2}$$

Thus, ψ_1, the compensation factor for the incident beam when it traverses any distance x, is

$$\psi_1 = e^{(\overline{\mu}_w - \overline{\mu}_0)x} = \left[e^{(\overline{\mu}_w - \overline{\mu}_0)d}\right]^{\frac{x}{d}} = \alpha^{\frac{x}{d}} \tag{3}$$

Similarly, the compensation factors for the scattered beam traversing a distance d (through the middle of a cord) and the factor for the distance x are

$$\frac{I_3(\overline{E}')}{I_2(\overline{E}')} = e^{(\overline{\mu}'_w - \overline{\mu}'_0)d} = \beta \tag{4}$$

$$\psi_2 = e^{(\overline{\mu}_w - \overline{\mu}_0)x} = \left[e^{(\overline{\mu}'_w - \overline{\mu}'_0)d}\right]^{\frac{x}{d}} = \beta^{\frac{x}{d}} \tag{5}$$

Note that these factors are functions of attenuation coefficients of the cord and rubber, and the cord diameter, but not functions of the distance from the sample entering position to the scatter site. Here the constants α and β are determined experimentally, while x can be calculated from the available geometric data. However, since the scatter angles are not uniform in the ComScan data acquisition geometry, the effective energies corresponding to each depth (layer) are all different. Scattered beams at different layers will then experience different amounts of attenuation. Thus, β should be measured at every scatter angle for an accurate reconstruction. This simple compensation method could eliminate all attenuation artifacts by the incident and scattered beams.

In the derivation of equations (3) and (5), both incident and scattered beams are assumed to be well collimated pencil beams. But ComScan uses a slit collimated fan-beam geometry. To reduce the resulting error, multiple beams are traced from the scatter site to the detector. The average distance through the cord is used.

RECONSTRUCTION

The reconstruction process utilizes results obtained in previous section. After an object is scanned, the data are normalized against a calibration sample containing only the matrix material of the object. Since the matrix of the object and the calibration material are identical, the difference in intensities will be shown only in the regions where the density of the object differs from that of the calibration material, and/or where the beam traverses through the difference region (cord). When the beam traverses the difference region, the length of the segment (x) traversing the region is calculated. With that information, compensation factors, ψ_1 and ψ_2, using

eq. (3) and eq. (5) are calculated and multiplied by the normalized data .

The reconstruction process works from the top layer to bottom layer as described in the previous report [7], but using the normalized data rather than the raw experimental data. In the first layer, all voxels are determined to belong to either the cord or the matrix using a certain criterion such as a threshold. This information is kept in an array to be used for the reconstruction of lower layers. From the second layer down, the beam paths are accurately traced to identify whether the beam traverses through any voxels whose densities are different from the calibration sample. If different, adjustment on their intensities is made first, then the densities are computed. The information obtained in the current layer is then used to reconstruct the next layer. This process continues until the densities of the deepest layer are obtained.

EXPERIMENT

A simple phantom was fabricated by casting a plastic resin containing an actual steel cord (radius of 0.74 mm) used in SRD construction. Only a single cord was positioned in the plastic matrix. The phantom was scanned so that the cord was parallel to the x-ray beam sweeping direction. A reference scan was performed with a solid plastic block as calibration material. 10 mm focal apertures and a 10 mm spacing between the scanner head and the phantom were used. The data were saved in a Bernoulli diskette and ported to an SGI workstation for the reconstruction.

Fig. 2 shows tomographs of the phantom along the z-axis. Attenuation (shadow) artifacts are visible in the images corresponding to the depth below the cord. Notice that the densities do not decrease gradually with depth due to the variations of detector efficiencies and other data acquisition variables. As expected, the scattered beams are attenuated more than the incident beams. The shadows caused by the scattered beams are slightly larger due to the scattered beam divergence.

Experimental data were normalized with the data obtained from a block of plastic. These are displayed as cross-sectional images along the Z-axis in Fig. 3. Note that the inconsistency due to variation in detector efficiencies was removed. To obtain the values of α and β needed for reconstruction, one has to acquire the data corresponding to the shadows, but this is difficult to do directly from the data. This process was facilitated by visually displaying the data as cross-sectional images and interactively plotting density profiles across the cord. The minimum values at two different dips, corresponding to attenuation through the center of the cord, were obtained seven times per image and averaged to reduce experimental errors.

As expected, the attenuation by the incident beam was uniform regardless of the depth. While the attenuation by the scattered beam was supposed to increase with depth, since the scatter beam loses more energy as the scatter angle increases, there was no measurable decrease in attenuation. This is probably due to the small differences in scatter angle (approximately 10°) between the first and the last layers when a 10 mm focal aperture is used, and the differences were within the statistical error. From these data, α and β were 1.66 and 2.14. These values were used for reconstruction.

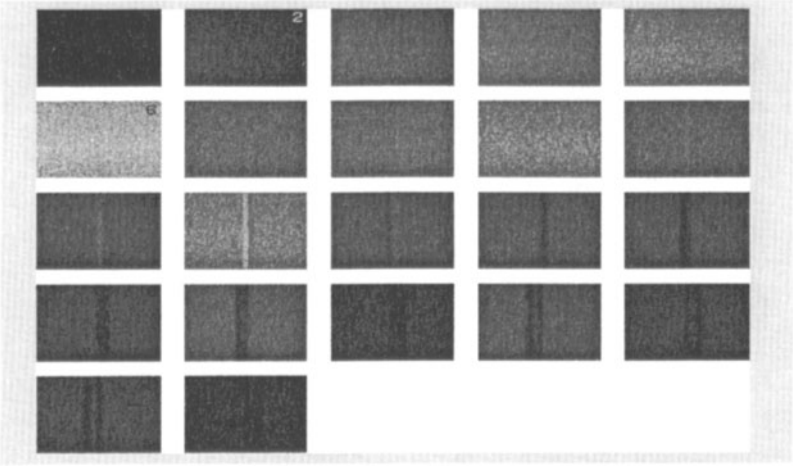

Figure 2: Raw data from a single cord phantom. Attenuation (shadow) artifacts are visible in the images corresponding to the depth below the cord. Notice the unusual brightness fluctuation between images due to the variations in detector efficiencies and other data acquisition variables.

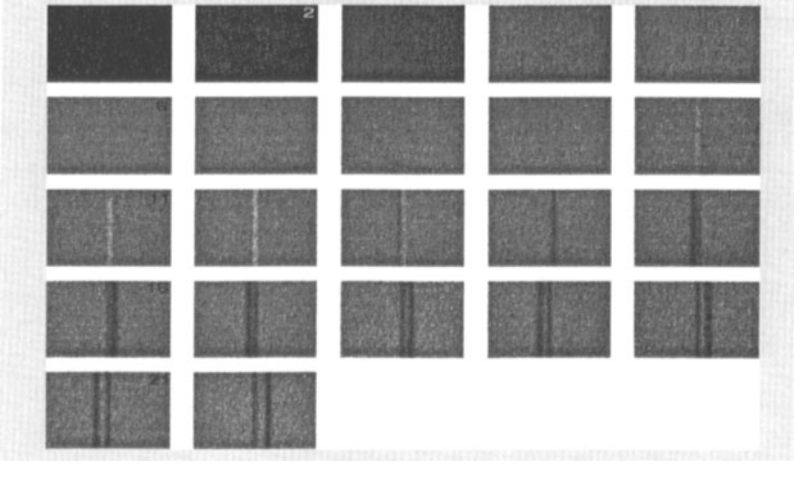

Figure 3: Normalized images: The brightness anomaly shown in Figure 2 is removed.

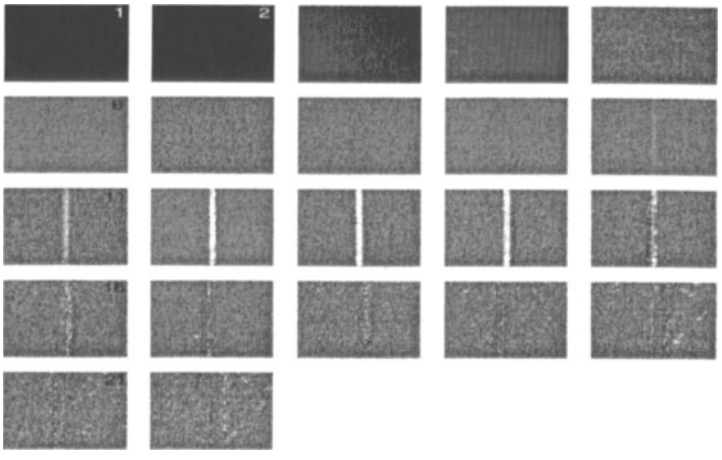

Figure 4: Reconstructed images: The normalized data are used for reconstruction. The shadows shown in Figure 3 are disappeared.

The reconstructed results are shown in Fig. 4. The attenuation artifacts shown in the raw data are almost gone, although some vestiges remain. A 3-D representation of the reconstruction is shown in Fig. 5.

CONCLUSION

We have developed a semi-empirical methodology to reconstruct data from a real x-ray backscatter inspection system with a particular application to the reconstruction of the SRD material. The methodology was successfully demonstrated by applying the algorithm to the data obtained from ComScan. One of the main difficulties of the reconstruction of the SRD is that the radius of cord is comparable to the size of a pixel. Considering that the size of the cord was close to the resolution of the scanner, we think that the result is quite remarkable.

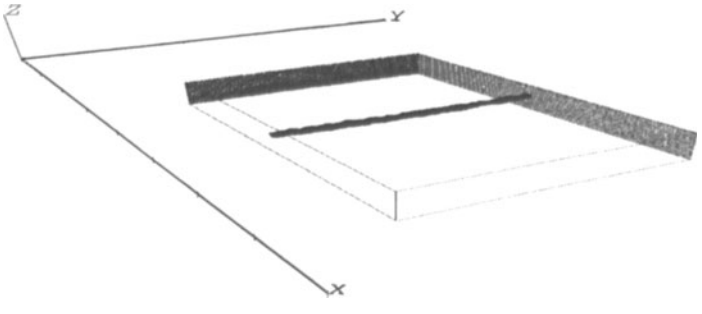

Figure 5: 3-D representation of the reconstructed results visualizing only the cord.

ACKNOWLEDGEMENTS

This work is supported by the Office of Naval Research Postdoctoral Fellowship, Exploratory Development Programs and the Naval Sea Systems Command.

REFERENCES

1. D.G. Costello, J.A. Stokes, and A.P. Trippe, "Theory and Applications of Collimated Photon Scattering," *14th Symposium on Nondestructive Evaluation*, San Antonio, TX, 1983
2. H. Strecker, "Scatter Imaging of Aluminum Castings Using an X-ray Fan Beam and a Pinhole Camera," *Materials Evaluation*, vol. 40, 1982
3. B.C. Towe and A.M. Jacobs, "X-ray Backscatter Imaging," *IEEE Transactions on Biomedical Engineering*, Vol. BME-28, No. 9, 1981
4. E.C. Greenawald, J.B. Nagode, C.F. Poranski, and Y.S. Ham "*In – Situ* NDE of Navy sonar Domes Via X-ray Backscatter Tomography," *Review of Progress in Quantitative NDE*, Vol. 14, p.881, 1995
5. G. Harding and J. Kosanetzky, "Scattered X-ray Beam Nondestructive Testing," Nucl. Instr. and Meth. in Phys. Res., Vol. A280, pp 517-528, 1989
6. E.C. Greenawald, Y.S. Ham, and C.F. Poranski, "Artifacts in X-ray Backscatter Tomography of Non-Homogeneous Objects," *Review of Progress in Quantitative NDE*, Vol. 13, 1994
7. Y.S. Ham, E.C. Greenawald, and C.F. Poranski, "Reconstruction Method for X-ray Backscatter Tomography," *Journal of the Canadian Society of Nondestructive Testing*, 1995 (To be published)